VCHP Performance Prediction: Comparison of First-Order and Flat Front Models

R. P. Bobco*
Hughes Aircraft Company, Los Angeles, California

Performance prediction equations are presented for a variable conductance heat pipe (VCHP) that exhibits a flat front temperature profile: the active condenser is isothermal and the temperature decreases monotonically along the length of the inactive condenser. A numerical comparison of evaporator temperatures predicted by the flat front model and the earlier first-order model shows that the results are almost equal for a wide range of heat loads. The flat front model exhibits an anomaly for high-heat loads that push the front to the entrance of the reservoir ($L_c = 1.0$). It is concluded that the first-order formulation has a broader range of application, but that the flat front model can be used for heat loads that prevent the front location from exceeding $L_c = 0.9$.

Nomenclature

A_c = internal cross section for vapor/gas transport
A_r = reservoir external surface area for heat transfer
A_w = conduction cross section of wick plus wall
b^2 = $(h\ell_1/k_w)(S\ell_1/A_w)$, fin parameter (nondimensional)
h = condenser heat loss coefficient (convection plus linearized radiation)
k_w = thermal conductivity of pipe wall and wick structure
ℓ_1 = total condenser length
ℓ_c = length of active condenser (location of condensation front)
L_c = ℓ_c/ℓ_1, nondimensional length of active condenser
m_g = mass of noncondensable gas
M^* = $m_g R_g T_s/p_v(T_s)V_c$, nondimensional mass of noncondensable gas
$p_v(T)$ = saturated vapor pressure evaluated at temperature T
Q = heat load entering condenser
R_g = gas constant of noncondensable gas
S = pipe periphery
T = local axial temperature (absolute)
T_s = local environment temperature (absolute)
T' = first derivative of temperature with respect to ζ
T'' = second derivative of temperature with respect to ζ
U_r^* = $b_r^2 A_r/S\ell_1$, reservoir heat loss parameter (nondimensional)
V_c = $A_c\ell_1$, volume occupied by vapor/gas in total condenser section
V_r = reservoir volume
z = axial location
α_i = constant of integration
ζ = z/ℓ_1, nondimensional axial location
v_r = V_r/V_c, reservoir-to-condenser volume ratio
ϕ_i = $\{[p_v(T_e) - p_v(\bar{T}_i)]/p_v(T_s)\}(T_s/\bar{T}_i)$, nondimensional gas density
$\Delta\tau$ = $Q/hS\ell_1$, heat load parameter, deg C or K

Subscripts

1 = active condenser section
2 = inactive condenser section
f = flat front model
I = first-order model
r = reservoir

Received May 19, 1988; revision received Aug. 23, 1988.

*Senior Scientist, Thermophysics Department. Associate Fellow AIAA.

Introduction

RECENT comparisons of analytical predictions and observed experimental values[1,2] show that a relatively simple one-dimensional model can be used to calculate evaporator temperature and axial temperature profiles as a function of heat load leaving the evaporator section. In the second study,[2] it is noted that VCHP performance predictions appear to be reasonably insensitive to the details of an analytical model for the operating range and working fluids reported. The present study provides additional insight into the problem of VCHP performance prediction by comparing the first-order model[1,2] and a flat front model.

Analysis

The geometry examined here (Fig. 1) consists of a condenser section and a reservoir. A heat load Q enters the condenser section at $\zeta = 0$. Condensation is assumed to occur at a constant flux, $Q/S\ell_1 L_c$, in the region $0 < \zeta \leq L_c$ (active condenser) only. Energy is lost to the surroundings by convection and/or linearized radiation from the outer surface of the active condenser, and conducted axially in the pipe wall to the region $L_c < \zeta \leq 1$ (inactive condenser). The pipe is simply connected to a wicked gas reservoir that is assumed to be isothermal at the temperature of the end of the pipe $T(1)$. Energy is lost to the surroundings from the surfaces of both the inactive condenser and the reservoir by convection and/or linearized radiation. For reasons of mathematical and computational simplicity, the model does not include primary or secondary insulated transport sections on either end of the condenser; the reservoir is assumed to be unheated.

The VCHP performance problem requires the simultaneous solution of the evaporator temperature T_e and condensation front location L_c as a function of heat load Q for a specified set of parameters (geometry, working fluids, thermophysical properties, environment). The conservation principles, assumptions, working equations, and calculation techniques

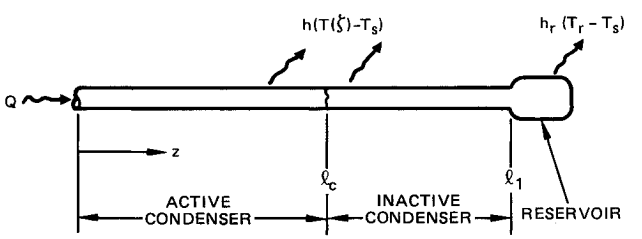

Fig. 1 VCHP geometry for both first-order and flat front formulations.

Table 1 Summary of analytical formulations for first-order and flat front models

Item	First-order model	Flat front model
Field equations	$T_1''(\zeta) - b^2[T_1(\zeta) - T_s] = -b^2\Delta\tau,\ 0 < \zeta \le L_c$	$T_2'(L_c) - b^2 L_c(T_e - T_s) = -b^2\Delta\tau,\ 0 < \zeta \le L_c$
	$T_2''(\zeta) - b^2[T_2(\zeta) - T_s] = 0,\ L_c < \zeta \le 1$	$T_2''(\zeta) - b^2[T_2(\zeta) - T_s] = 0,\ L_c < \zeta \le 1$
Boundary and matching conditions	$T_1'(0) = 0$	
	$T_1(L_c) = T_2(L_c),\ T_1'(L_c) = T_2'(L_c)$	$T_2(L_c) = T_e$
	$T_2'(1) = U_r^*[T_s - T_2(1)]$	$T_2'(1) = U_r^*[T_s - T_2(1)]$
Axial temperature solutions	$\dfrac{T_1(\zeta) - T_s}{\Delta\tau} = \dfrac{1}{L_c}(1 - \alpha_1 \cosh b\zeta),\ 0 < \zeta \le L_c$	$\dfrac{T_e - T_s}{\Delta\tau} = \dfrac{1}{L_c(1 + \gamma_c/bL_c)},\ 0 > \zeta \le L_c$
	$\dfrac{T_2(\zeta) - T_s}{\Delta\tau} = \dfrac{\alpha_2}{L_c}[U_r^* \sinh b(1-\zeta) +$ $b \cosh b(1-\zeta),\ L_c < \zeta \le 1$	$\dfrac{T_2(\zeta) - T_s}{\Delta\tau} = \dfrac{\alpha_3}{L_c}[U_r^* \sinh b(1-\zeta) +$ $b \cosh b(1-\zeta)],\ L_c < \zeta \le 1$
Mean temperature	$\dfrac{\bar{T}_1 - T_s}{\Delta\tau} = \dfrac{1}{L_c}(1 - \dfrac{\alpha_1}{bL_c} \sinh bL_c),\ 0 < \zeta \le L_c$	$\bar{T}_1 = T_e,\ 0 < \zeta \le L_c$
	$\dfrac{\bar{T}_2 - T_s}{\Delta\tau} = \dfrac{\alpha_2}{b(1-L_c)L_c}[U_r^*(\cosh b(1-L_c) - 1) +$ $b \sinh b(1-L_c)],\ L_c < \zeta \le 1$	$\dfrac{\bar{T}_2 - T_s}{\Delta\tau} = \dfrac{\alpha_3}{b(1-L_c)L_c}[U_r^*(\cosh b(1-L_c) - 1) +$ $b \sinh b(1-L_c)],\ L_c < \zeta \le 1$
Gas inventory	$L_{cI} = \dfrac{\phi_2 + \phi_r v_r - M^*}{\phi_2 - \phi_1}$	$L_{cf} = \dfrac{\phi_2 + \phi_r v_r - M^*}{\phi_2}$
Constants of integration	$\alpha_1 = [U_r^* \cosh b(1-L_c) + b \sinh b(1-L_c)]/D$	$\alpha_3 = \{[(1 + \gamma_c/bL_c)[U_r^* \sinh b(1-L_c) + b \cosh b(1-L_c)]\}^{-1}$
	$\alpha_2 = (\sinh bL_c)/D$	$\gamma_c = \dfrac{U_r^* \cosh b(1-L_c) + b \sinh b(1-L_c)}{U_r^* \sinh b(1-L_c) + b \cosh b(1-L_c)}$
	$D = U_r^* \cosh b + b \sinh b$	
Parameters	$b^2 = \dfrac{h\ell_1}{k_w}\dfrac{S\ell_1}{A_w},\quad U_r^* = \dfrac{h_r A_r \ell_1}{k_w A_w},\quad M^* = m_g R_g T_s/p_v(T_s)V_c,\quad v_r = V_r/V_c$	
	$\phi_i = \left[\dfrac{p_v(T_e) - p_v(\bar{T}_i)}{p_v(T_s)}\right]\left[\dfrac{T_s}{\bar{T}_i}\right],\quad \Delta\tau = Q/hS\ell_1$	

Table 2 Hypothetical VCHP dimensions, properties, and parameters

Materials	
Pipe	6061 T6 aluminum
Reservoir	304L stainless steel
Working fluid	NH_3 (anhydrous ammonia)
Noncondensable gas	N_2 (nitrogen)
Geometry	
Pipe o.d. × wall thickness	1.27 × 0.071 cm
Condenser length	$\ell_1 = 152.4$ cm
Pipe circumference	$S = 3.99$ cm
Conduction cross section	$A_w = 0.2679$ cm^2
Vapor cross section	$A_c = 0.5643$ cm^2
Reservoir surface area	$A_r = 157.9$ cm^2
Reservoir volume	$V_r = 252.4$ cm^3
Thermal coefficients	
Pipe thermal conductivity	$k_w = 171.3$ w/m-k
Condenser section	$h = 11.15$ w/m^2-k
Reservoir	$h_r = 11.15$ w/m^2-k
Gas charge	
Mass	$m_g = 3.577 \times 10^{-3}$ kg
Gas constant	$R_g = 0.2968$ kJ/kg-K
Boundary temperature	$T_s = 294.4$ K

have all been described.[1,2,3] The essential features of a flat front VCHP model are the assumptions of 1) negligible noncondensable gas in the active condenser and 2) an isothermal active condenser section. Table 1 presents the heat and mass balance equations and their solutions for both first-order and flat front VCHP models. For each model, the working equations consist of the following: evaporator temperature $T_1(0) = T_e$; active and inactive condenser mean temperature $\bar{T}_1$ and $\bar{T}_2$; reservoir temperature $T_2(1) = T_r$; condensation front location L_c; and a correlation[4] for vapor saturation pressure as a function of temperature, $p_v(T) = \exp[f(T)]$. Insofar as the temperature equations are transcendental in L_c and $p_v(T)$ is a transcendental/nonlinear function of temperature, an iterative numerical procedure is required to solve for T_e and L_c.

Numerical Results

With the exception of the working fluid properties, the parameters that influence VCHP performance have been reduced to four nondimensional groups: b, U_r^*, v_r, M^*. A hypothetical VCHP, described previously,[2] was used to select a baseline for comparing the two analytical models. The essential features of the heat pipe are summarized in Table 2. The geometry and properties are similar to those of VCHP's for space applications, but the environment corresponds to free convection/radiation in shirt-sleeve surroundings. The

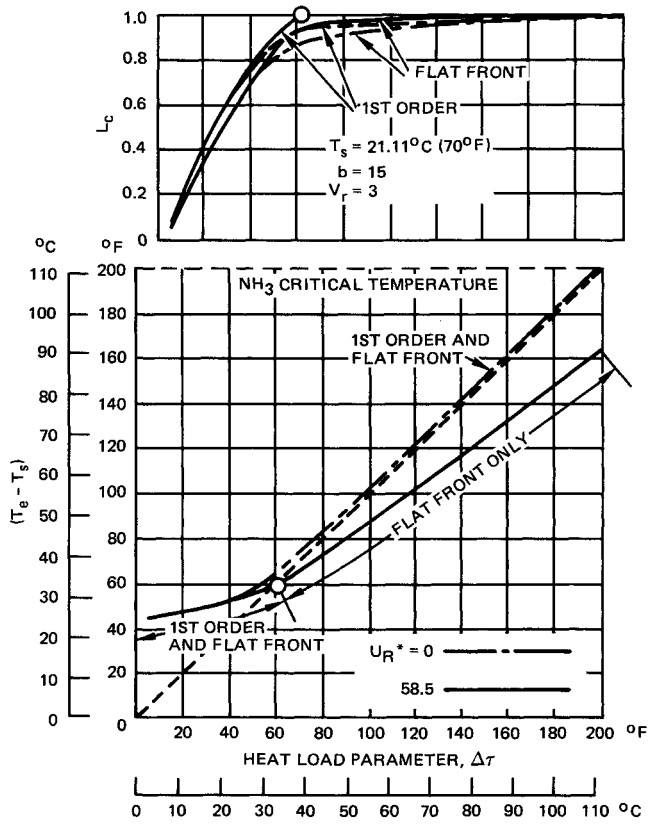

Fig. 2 Comparison of VCHP evaporator temperatures and condensation front locations for first-order and flat front models with adiabatic and convectively cooled reservoirs.

Table 3 Influence of ±5% error in gas inventory on evaporator temperature

	First-order			Flat front			
Δτ, °C	L_c	T_e, °C	T_r, °C	L_c	T_e, °C	T_r, °C	Comment
11.111	0.39283	49.310	21.112	0.33025	49.105	21.112	0.95 L_c
11.111	0.41351	47.927	21.112	0.34763	47.931	21.112	Baseline
11.111	0.43419	46.663	21.112	0.36501	46.851	21.112	1.05 L_c
22.222	0.72635	51.705	21.214	0.66320	51.558	21.191	0.95 L_c
22.222	0.76458	50.176	21.284	0.69811	50.168	21.239	Baseline
22.222	0.80281	48.792	21.404	0.73302	48.899	21.318	1.05 L_c
33.333	0.93908	56.607	24.016	0.87920	56.273	23.493	0.95 L_c
33.333	0.98851	54.832	26.903	0.92547	54.407	25.854	Baseline
33.333	1.03794	52.860	34.807	0.97174	51.870	32.119	1.05 L_c

Table 4 Influence of variations in b, v_r, and M^* on evaporator temperature: nonadiabatic reservoir

				First-order			Flat front		
Δτ, °C	b	v_r	M^*	L_c	T_e, °C	T_r, °C	L_c	T_e, °C	T_r, °C
5.556	12	3	4.17456	0.19514	46.843	21.112	0.13264	46.834	21.112
	15[a]	3	4.17456	0.20602	46.851	21.111	0.14920	46.847	21.112
	18	3	4.17456	0.21094	46.857	21.111	0.16024	46.856	21.112
27.778	12	3	4.17456	0.89588	52.117	23.268	0.81688	51.932	22.784
	15[a]	3	4.17456	0.90398	51.839	22.597	0.84041	51.712	22.257
	18	3	4.17456	0.90924	51.662	22.161	0.85599	51.571	21.917
55.556	12	3	4.17456	—	—	—	0.97974	69.834	48.243
	15[a]	3	4.17456	—	—	—	0.98674	69.784	48.141
	18	3	4.17456	—	—	—	0.99067	69.756	48.084
5.556	15	2	4.17456	0.15698	53.142	21.111	0.10685	53.129	21.111
	15	4	4.17456	0.25166	42.681	21.111	0.19092	42.679	21.111
27.778	15	2	4.17456	0.73851	58.724	21.298	0.67174	58.729	21.249
	15	4	4.17456	—	—	—	0.93746	48.374	25.252
55.556	15	2	4.17456	—	—	—	0.96728	73.303	40.856
	15	4	4.17456	—	—	—	0.99237	67.329	50.957
5.556	15	3	3.74271	0.22621	44.845	21.111	0.16744	44.842	21.111
	15	3	4.60641	0.18900	48.779	21.111	0.13417	48.792	21.111
27.778	15	3	3.74271	0.94629	50.466	23.788	0.88429	50.245	23.247
	15	3	4.60641	0.86044	53.394	21.923	0.79536	53.328	21.723
55.556	15	3	3.74271	—	—	—	0.98885	69.273	49.996
	15	3	4.60641	—	—	—	0.98434	70.306	46.308

[a]Baseline conditions.

Table 5 Influence of variations in b, v_R, and M^* on evaporator temperature: adiabatic reservoir

				First-order			Flat front		
$\Delta\tau$, °C	b	v_r	M^*	L_c	T_e, °C	T_n, °C	L_c	T_e, °C	T_r, °C
5.556	12	3	4.17456	0.19513	46.844	21.111	0.13263	46.835	21.111
	15[a]	3	4.17456	0.20600	46.851	21.111	0.14920	46.847	21.111
	18	3	4.17456	0.21094	46.857	21.111	0.16024	46.856	21.111
27.778	12	3	4.17456	0.84961	53.804	26.491	0.77819	53.384	25.596
	15[a]	3	4.17456	0.86455	53.241	25.323	0.80714	52.916	24.625
	18	3	4.17456	0.87551	52.839	24.486	0.82742	52.578	23.922
55.556	12	3	4.17456	0.96837	78.481	60.362	0.92030	77.674	58.989
	15[a]	3	4.17456	0.97412	78.143	59.794	0.93578	77.484	58.668
	18	3	4.17456	0.97809	77.911	59.402	0.94622	77.354	58.450
5.556	15	2	4.17456	0.15698	53.142	21.111	0.10685	53.129	21.111
	15	4	4.17456	0.25166	42.681	21.111	0.19092	42.679	21.111
27.778	15	2	4.17456	0.73422	58.933	21.815	0.66887	58.886	21.637
	15	4	4.17456	0.91922	51.330	30.107	0.86906	50.879	29.302
55.556	15	2	4.17456	0.95630	79.206	51.271	0.91159	78.416	49.536
	15	4	4.17456	0.98165	77.706	64.085	0.94726	77.160	63.267
5.556	15	3	3.74271	0.22620	44.845	21.111	0.16744	44.842	21.111
	15	3	4.60641	0.18900	48.779	21.111	0.13417	48.773	21.111
27.778	15	3	3.74271	0.89047	52.306	27.144	0.83610	51.914	26.344
	15	3	4.60641	0.83519	54.370	23.918	0.77490	54.124	23.364
55.556	15	3	3.74271	0.97741	77.951	61.614	0.94060	77.338	60.599
	15	3	4.60641	0.97064	78.347	57.958	0.93088	77.647	56.724

[a]Baseline conditions.

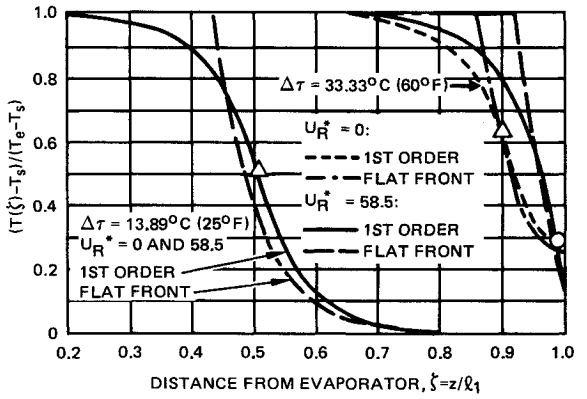

Fig. 3 Temperature profiles for first-order and flat front models: two heat loads and two gas reservoir conditions.

baseline values are $b = 15$, $U_r^* = 58.5$, $v_r = 3$, and $M^* = 4.175$. A set of limited variations among these nondimensional groups was examined to determine the influence of such variation on evaporator and reservoir temperatures and on condensation front location. A major variation based on $U_r^* = 0$ (adiabatic reservoir) and $U_r^* = 58.5$ was examined, with selected variations in $b(=12, 18)$, $v_r(=2, 4)$, and $M^*(=3.7427, 4.6064)$. For the nonadiabatic reservoir cases, U_r^* was recast as a function of b and v_r to account for variations in environmental conditions, reservoir size, etc.; the working relationship was taken as $U_r^* = b^2 v_r^{2/3}/8$. The expression for U_r^* followed from the definition of U_r^*, the baseline geometry, and the assumption that reservoir surface area A_r varies as $V_r^{2/3}$. The heat load parameter $\Delta\tau = Q/hS\ell_1$ was treated as the independent variable of the performance problem, and calculations were made for the range 2.78°C (5°F) $\leq \Delta\tau \leq$ 111.11°C (200°F). The upper limit on $\Delta\tau$ corresponds to the critical temperature of ammonia; the lower limit was selected to avoid specifying geometry and conditions upstream ($z < 0$) of the condenser section. The saturated vapor pressure of ammonia was calculated from a polynomial expression.[4] The closed-form working equations were coded for a hand calculator, and an iterative procedure[1,2] was used to obtain simultaneous solutions for T_e and L_c. The performance results are presented in Fig. 2 and in Tables 3, 4, and 5. Nondimensional temperature profiles for two values of $\Delta\tau$ are shown for both VCHP models in Fig. 3.

Discussion

The heat load parameter $\Delta\tau$ has the dimension of temperature and it represents the temperature, above ambient, that an ideal fixed conductance heat pipe (FCHP) would experience for the specified heat load. An ideal FCHP is isothermal in the absence of internal pressure drops, liquid puddles, wick dryout, and similar real effects. The heat load parameter arises in a natural way in the course of the mathematics and it provides a convenient link for comparing VCHP and FCHP performance.

Fig. 2 shows that both models predict virtually identical values of evaporator temperature for both reservoir conditions at nominal heat loads [2.78°C (5°F) $\leq \Delta\tau \leq$ 22.22°C (40°F)]. The flat front model predicts a lower value of L_c than the first-order model in this $\Delta\tau$ range, but the influence on evaporator temperature is negligible. Evaporator temperature deviations occur among the several cases for values of $\Delta\tau >$ 22.22°C (40°F); these cases are discussed individually below.

1) *First-order model, $U_r^* = 58.5$:* The condenser length is completely utilized ($L_{c,1} = 1.0$) at a heat load parameter value $\Delta\tau$ = 34.5°C (62.1°F). The evaporator and reservoir temperature ranges corresponding to 2.78°C $\leq \Delta\tau \leq$ 34.5°C are 46.32°C (115.37°F) $\leq T_e \leq$ 55.62°C (132.11°F) and 21.11°C (70°F) $\leq T_r \leq$ 28.14°C (82.65°F). The analytical model is incapable of predicting VCHP performance for higher heat loads ($L_{c,1} \geq 1.0$).

2) *Flat front model, $U_r^* = 58.5$:* In the operating range of the preceding first-order model, the flat model predicts evaporator and reservoir temperatures that are lower by 0.43°C (0.77°F) and 2.29°C (4.12°F) at $\Delta\tau$ = 33.33°C (60°F); the flat front location is $L_{c,f} = 0.9255$. The flat front model predicts that much higher heat loads can be accommodated before the full condenser length is used; at $\Delta\tau$ = 111.11°C (200°F), the flat front performance is ($L_{c,f}$, T_e, T_r) = (0.9974, 111.77°C, 99.84°C). It is important to note that the flat front model leads to an anomaly as $L_{c,f} \to 1.0$ because the assumption $T_r = T(1)$ implies $p_v(T_r) \to p_v(T_e)$ and $m_g \to 0$.

3) *First-order model, $U_r^* = 0$:* The influence of an adiabatic reservoir is imperceptible for $\Delta\tau <$ 22.22°C (40°F). At $\Delta\tau$ = 33.33°C (60°F), the model predicts $L_{c,1} = 0.91651$, and

T_e and T_r are 2.65°C (4.77°F) and 4.60°C (8.28°F) higher, respectively, than the case with $U_R^* = 58.5$. It was found that the noncondensable gas anomaly occurs for the first-order model with an adiabatic reservoir; additionally, it was found that, as $L_{c,I} \to 1.0$, the evaporator temperature approaches the critical temperature of NH_3 (132.4°C). It is believed that the predictions are of academic interest only for heat loads that lead to $L_{c,I} > 0.9$; calculations for $\Delta\tau = 55.56$°C (100°F) yield $(L_{c,I}, T_e, T_r) = (0.9741, 78.14$°C, 59.79°C).

4) *Flat front model, $U_r^* = 0$:* This case is barely different from the first-order model with adiabatic reservoir. The predicted performance at $\Delta\tau = 55.56$°C (100°F) is $(L_{c,f}, T_e, T_r) = (0.9358, 77.48$°C, 58.67°C). The anomalies in mass inventory and critical temperature occur, also, as $L_c \to 1.0$.

An unexpected finding of this first-order/flat front model comparison is the closeness of evaporator temperatures as a function of heat load predicted by the two formulations. The first-order and flat front predictions for condensation front location L_c are dissimilar, in general, but the evaporator temperatures are comparable for all engineering applications.

The low sensitivity of evaporator temperature to L_c is remarked upon by Bobco.[2] Similar results are summarized in Table 3 for both models with nonadiabatic reservoirs. An error of $\pm 5\%$ in L_c produced errors in evaporator temperature of approximately ± 1.3°C (2.3°F) for $\Delta\tau = 11.11$°C (20°F) and ± 2.0°C (3.6°F) for $\Delta\tau = 33.33$°C (60°F). The temperature errors are not negligible, but they are acceptable for most engineering applications. Once again, it appears possible to predict VCHP temperature performance without precise adherence to the constraint imposed by the noncondensable gas inventory.

Table 4 summarizes performance data (L_c, T_e, T_r) for first-order and flat front models with nonadiabatic reservoir and shows the influence of variations in b, v_r, and M^*; Table 5 contains the same information for an adiabatic reservoir. For the range of parameters shown, it can be seen that evaporator temperature has a slight sensitivity to the model and to the fin parameter b; a greater sensitivity to the gas mass parameter M^*; and a pronounced sensitivity to the reservoir/pipe volume ratio v_r.

Figure 3 shows nondimensional axial temperature profiles for the two analytical models, with both adiabatic and nonadiabatic reservoirs at two-heat loads. At $\Delta\tau = 13.89$°C (25°F), the temperature distribution is independent of the reservoir heat loss parameter (U_r^*). At the higher heat load, $\Delta\tau = 33.33$°C (60°F), the temperature profiles are different and distinct among the four cases. In general, the reservoir temperature is seen to depend on the reservoir heat loss parameter more than on the analytical model; for a given U_r^*, the flat front model predicts a lower temperature than does the first-order model.

The anomaly associated with $L_c \to 1.0$ identifies the need for a more sophisticated model of heat and mass transport in the reservoir volume. A refined reservoir model is required both for heat loads that cause $L_c \to 1.0$ and very high loads that cause condensation to occur within the reservoir. A more sophisticated reservoir model must account for the possibility of free convection and/or mass diffusion in the reservoir volume and must include a validated criterion for selecting the region of the reservoir surface on which condensation occurs. Such a reservoir would not be isothermal (unless it were adiabatic) and would avoid the anomaly implicit in the present model that assumes $T_r = T(1)$.

Of the two VCHP models, and the two reservoir conditions examined here, only the first-order model with nonadiabatic reservoir did not exhibit the anomaly as $L_c \to 0$. For this case, the maximum value of the heat load parameter was found to be $\Delta\tau = 34.5$°C. This value is credible, but it must be recognized that it is approximate. In general, limiting conditions are sensitive to the assumptions implicit in an analytical model. Intuition suggests that consideration of two-dimensional effects at the condensation front and more realistic conditions in the reservoir will influence the magnitude of the maximum value of heat load parameter.

Conclusions

Comparison of two different VCHP formulations demonstrates that both the flat front and first-order models predict nearly identical values of evaporator temperature for a wide range of heat loads. The first-order formulation provides credible performance predictions for all conditions, except the case of an adiabatic gas reservoir ($U_r^* = 0$). The adiabatic reservoir leads to an anomaly for high-heat loads that drive the condensation front to the entry of the reservoir ($L_c = 1.0$). The flat front formulation exhibits the same anomalous behavior for all values of $U_r^* \geq 0$. It is concluded that the first-order model is applicable over a broader range of heat loads than the flat front model, and that the flat front model should be restricted to the case of heat loads that prevent the condensation front from exceeding $L_c = 0.9$.

References

[1]Bobco, R. P., "Variable Conductance Heat Pipes: A First-Order Model," *Journal of Thermophysics and Heat Transfer*, Vol. 1, Jan. 1987, pp. 35–42.

[2]Bobco, R. P., "An Extended Model for VCHP Analysis: Zero-to-Full Heat Loads," AIAA Paper 87-1614, June 1987; also, *Journal of Thermophysics and Heat Transfer* (to be published).

[3]Edwards, D. K. and Marcus, B. D., "Heat and Mass Transfer in the Vicinity of the Vapor Gas Front in a Gas Loaded Heat Pipe," *Journal of Heat Transfer*, Vol. 94C, No. 2, May 1972, pp. 155–162.

[4]Brennan, P. J. and Kroliczek, E. J., "Heat Pipe Design Handbook," NASA Goddard Space Flight Center, Greenbelt, MD, Contract NAS5-23406, June 1979.